Power performance and dynamic responses of a combined floating vertical axis wind turbine and wave energy converter concept

Zhengshun Cheng[1,2], Ting Rui Wen[3], Muk Chen Ong[3], Kai Wang[4*]

1 Department of Marine Technology and AMOS, Norwegian University of Science and Technology, 7491 Trondheim, Norway.

2 State Key Laboratory of Hydraulic Engineering Simulation and Safety, Tianjin University, Tianjin, China.

3 Department of Mechanical and Structural Engineering and Materials Science, University of Stavanger, 4036 Stavanger, Norway.

4 Aker Solutions AS, 1366 Lysaker, Norway.

*Correspondence author. Email: wangkai.ntnu@gmail.com

Abstract

Currently, the development of floating wind turbines and wave energy converters (WECs) is both facing the challenge of high cost-of-energy (CoE). A promising way to reduce the CoE is to employ combined wind and wave energy concepts because they can share the same floating platform, mooring systems, and electrical cables and thus reduce the construction cost. Several combined concepts with floating horizontal axis wind turbines (HAWTs) have been proposed and studied. Compared to floating HAWTs, floating vertical axis wind turbines (VAWTs) have a good potential for CoE reduction. Therefore, this study proposes a novel combined wind and wave energy concept, which consists of a spar-type floating VAWT and a torus-shaped point absorber WEC. This combined concept utilizes the relative heave motion between the torus and the spar buoy to harvest wave energy. Fully coupled simulations under turbulent wind and irregular waves are carried out to evaluate its power performance and to assess the effect of the additional torus on the dynamic behavior of the floating VAWT. The results indicate that introducing the WEC contributes to the total power production while causing limited impacts on the power production and dynamic responses of the floating VAWT. The proposed combined concept is promising.

Keywords: floating vertical axis wind turbine; wave energy converter; combined concept; power performance; dynamic response.

1 Introduction

In recent years offshore wind power has been increasing rapidly, and offshore wind farms are moving towards deep water where floating offshore wind turbines are favorable. Wind turbines are usually categorized into horizontal axis wind turbines (HAWTs) and vertical axis wind turbines (VAWTs). Floating HAWTs have been widely studied and several prototypes of floating HAWTs have been deployed and tested, such as the Hywind demo in Norway, the WindFloat demo in Portugal, the VolturnUS turbine off the coast of Maine in the USA, the floating wind turbines off the Fukushima coast in northeast Japan and off the Goto island in southwest Japan, and the IDEOL floating wind turbine in France. Moreover, the world's first commercial floating wind farm, i.e., the Hywind Scotland by Equinor (previously known as Statoil), has started its power production in 2017.

Floating HAWTs are facing the challenge of high cost-of-energy (CoE)[1]. Floating VAWTs have a great potential to reduce the CoE [2] and are thus a promising alternative to floating HAWTs in the future floating wind market. Apart from that, floating VAWTs have many other advantages [3]. They are independent of wind direction, which implies that the yaw control system is not needed. The heavy components, e.g., generator, can be placed at the tower base which is favorable for operation and maintenance.

Compared to floating HAWTs, the development of floating VAWTs is still at an early stage. Many efforts have been devoted by researchers to demonstrate the dynamic response characteristics of various floating VAWT concepts. A novel concept with a two-bladed Darrieus rotor and a rotating spar buoy was proposed and extensively studied in the DeepWind project [4,5]. Borg and Collu [6] studied the aerodynamic characteristics of a semi-submersible type VAWT in the frequency domain. Wang et al. [7] developed a fully coupled simulation tool, i.e., SIMO-RIFLEX-DMS, for numerical modeling and dynamic analysis of floating VAWTs. This simulation tool was later applied to reveal the dynamic responses of a semi-submersible type VAWT [8]. Cheng et al. [9] developed another fully coupled tool for integrated dynamic analysis of floating VAWTs and conducted a series of studies to demonstrate the effects of floating supporting structures [10], blade number [11] and rotor optimization [12]. Liu et al. [13] conducted a numerical and experimental study on the motion of a 5 MW floating VAWT in which a truss spar floating foundation with heave plates is used.

Besides offshore wind energy, ocean wave energy is also a kind of marine renewable energies and has attracted great interest from both the industry and the research community. Numerous studies on converting wave energy into reliable power have been carried out all over the world. French [14] identified several types of wave energy converters (WECs) that are considered as promising solutions with higher economic values. A detailed evaluation of eight WEC concepts to identify their power

performance and annual absorbed energy was conducted by Babarit et al. [15] through numerical simulations. Muliawan et al. [16] performed a numerical analysis of a floating two-body wave energy converter, which consists of a torus, a floater, the power take-off (PTO) system and the mooring system. The effects of mooring configurations and PTO parameters on the energy absorption were assessed. Although many WEC concepts have been proposed, few are commercialized due to the relatively low efficiency and the high CoE.

To lower the cost, alternative solutions, e.g., integration of a floating wind turbine and a wave energy converter, have been proposed. In such integrated concepts, the wind turbine and the wave energy converter can share the same floating platform, mooring systems, and electrical cables. This basic idea is to save not only the workspace but also the construction cost. Several integrated concepts have been proposed in the European project MARINA Platform [17] which is dedicated to develop the integrated offshore wind and wave energy systems and rendering their applications closer to the market requirements. These concepts include a combination of semi-submersible type floating HAWT and flap-type wave energy converter [18,19], a combination of spar-type HAWT and a torus-shaped wave energy converter (STC) [20–22], and an oscillating water column wave energy converter on a floating foundation WindFloat [23].

The STC (spar-torus-combination) concept consists of one spar buoy supporting the HAWT, one torus-shaped floater, a PTO system and a catenary mooring system. The offshore wind energy is captured by the wind turbine, and the wave energy is absorbed through the PTO system via a relative heave motion between the torus and the spar buoy. The STC concept is suitable for the deployment in deep water, and it is not sensitive to seabed conditions or wave directions [20]. The dynamic response and power performance of the STC concept under operational modes and survival modes were numerically studied by Muliawan et al. [21,22]. Wan et al. [24,25] carried out a numerical and experimental study of hydrodynamic responses for the STC concept. To assess its long-term performance, two additional survival modes were proposed, and the power production, structural fatigue damage, and extreme responses were also investigated by Ren et al. [26].

Owing to the potential of floating vertical axis wind turbines (VAWTs), a combination of a floating VAWT and a WEC is also of great interest and is worth conducting numerical investigations and evaluations. In this study, a novel combined floating VAWT and WEC concept is proposed. This concept is inspired by the STC concept proposed by Muliawan et al. [20] and also by the successful experience of operation and production of spar-type HAWTs in the Hywind Scotland project. Power performance and stochastic dynamic response characteristics of the novel combined concept is numerically assessed by fully coupled time domain simulations under turbulent wind and irregular waves. The advantages and disadvantages of the concept are discussed and compared with a spar-type VAWT, which was

proposed by Cheng et al. [3].

2 A combined wind and wave energy concept

The present study proposes a combined wind and wave energy concept, as shown in Fig. 1. It combines a spar-type vertical axis wind turbine and a torus-shaped wave energy converter. Therefore, this novel concept is also denoted as STC (spar-torus-combination). This concept is initially inspired by the concept proposed by Muliawan et al. [20–22], which combines a spar-type floating horizontal axis wind turbine and a torus-shaped wave energy converter.

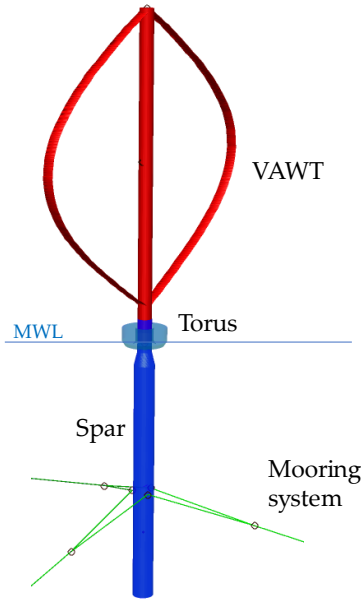

Fig. 1 Illustration of the combined wind and wave energy concept STC. It consists of a spar-type vertical axis wind turbine and a torus-shaped wave energy converter.

This novel concept includes a 5MW Darrieus-type vertical axis wind turbine, a torus-shaped wave energy converter, a spar buoy and a mooring system. The VAWT generates power from the wind and is supported by the spar buoy. The torus is a self-reacting point absorber that primarily operates in the heave mode. In the combined concept, the torus and spar buoy are two concentric floaters. The torus will slide along the spar buoy to extract energy from waves. The conceptual sketch is shown in Fig. 1, and its detailed configuration is displayed in Fig. 2. The considered water depth is assumed to be 320m.

The most prominent character of this concept is that the torus makes use of the spar buoy designed for the VAWT to capture wave energy. In this way, the wind turbine and the wave energy converter utilize the same floating platform, implying that more energy can be captured. At the same time,

introducing the torus may affect the dynamic responses of the spar-type VAWT, which should be properly assessed. Therefore, this study aims to reveal the power performance improvement by introducing the wave energy converter and its effect on the dynamic responses of the spar-type VAWT.

The detailed components and mechanisms for this combined concept are introduced in the following sections.

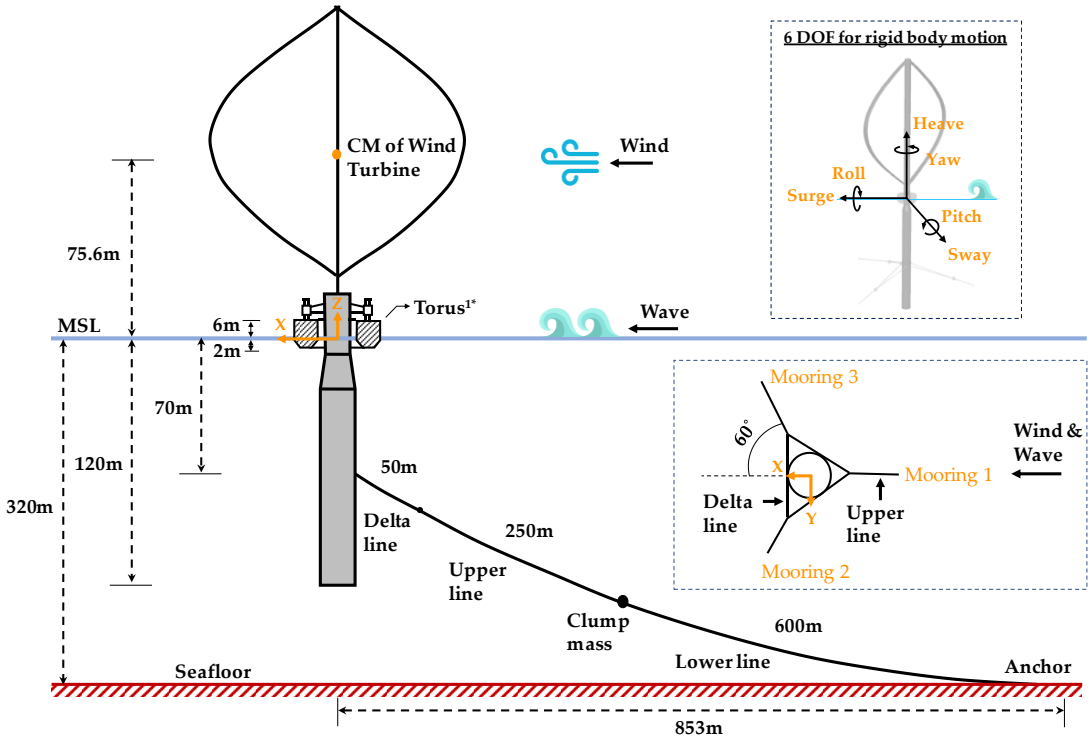

Fig. 2. The sketch of the combined wind and wave energy concept STC. It should be noted that the dimensions are not in the same scale. Detailed connections can be referred to Fig. 3, and CM denotes center of mass and MSL denotes the mean sea level.

2.1 Spar-type VAWT

The spar-type VAWT concept was developed by Cheng et al. [10]. In this concept, a spar buoy is used to support a 5MW Darrieus-type VAWT. Heavy ballast is placed at the bottom of the spar buoy to limit the platform pitch and roll motions under wind and wave conditions. The horizontal restoring stiffness is provided by the catenary chain mooring system, in which delta lines and clump weights are applied to increase the yaw stiffness to resist the aerodynamic yaw moment. Main properties of the mooring system are given in Table 3.

The rotor was originally developed in the DeepWind project [5]. Main specifications of the rotor are provided in Table 1. The rotor comprises two blades and one rotating tower that spans from top to

bottom. The bottom, located close to the mean sea level, is connected to a direct drive generator. The spar buoy was developed by Cheng et al. [10] based on the OC3 spar buoy [27], which was originally used to support the NREL 5MW horizontal axis wind turbine [28]. Due to the difference in rotor mass between the NREL 5MW wind turbine and the 5MW Darrieus rotor, the ballast of the spar buoy considered was slightly adjusted to achieve the same draft and displacement as the OC3 spar buoy. Since the difference in rotor mass was small compared to the displacement of the spar buoy, it was assumed that such adjustment does not significantly alter the hydrostatic performance. The geometrical and structural properties of the spar buoy are given in Table 2. This spar-type VAWT has been extensively studied by Cheng et al. [3,10] and Wen et al. [29].

Table 1 Main specifications of the Darrieus 5 MW wind turbine [4]

Item	Unit	Value
Rated power	[MW]	5
Rotor height, root to root	[m]	129.56
Rotor radius	[m]	63.74
Chord length	[m]	7.45
Airfoil section	[-]	NACA 0018
Cut-in, rated, cut-out wind speed	[m/s]	5, 14, 25
Rated rotational speed	[rpm]	5.26
Total mass, incl. rotor and tower	[kg]	754226
Center of mass	[m]	(0,0,75.6)

Table 2 Main properties of the spar buoy [10]. Note that Center of Mass (COM) only includes the contribution from spar, ballast, and generator. COB denotes the center of buoyancy and MSL represents the mean sea level.

Item	Unit	Value
Water depth	[m]	320
Draft	[m]	120
Waterline diameter	[m]	6.5
Diameter at bottom	[m]	9.4
Hull mass, including ballast and generator	[ton]	7308.3
COM location below MSL	[m]	-89.76
Displacement	[m^3]	8027
COB location below MSL	[m]	-62.06
Mass moment of inertia in roll and pitch, I_{XX} and I_{YY}	[ton·m^2]	6.362×10^7
Mass moment of inertia in yaw, I_{ZZ}	[ton·m^2]	1.588×10^5

Table 3 The properties of mooring system components [27]

Component	Length [m]	Mass [kg/m]	Axial stiffness [kN]
Delta line	50	42.5	200,000
Upper line	250	42.5	80,000
Clump mass	2	17,253	80,000
Lower line	600	42.5	60,000

2.2 Torus-shaped wave energy converter

The torus is a ring-shaped axisymmetric buoy that floats on the sea surface. Under the wave action, the torus will slide along the spar buoy, causing relative heave motion between the spar buoy and the torus. This relative heave motion will be utilized for wave energy extraction by the PTO system that is deployed between the spar buoy and the torus. The torus considered is the same as those used by Muliawan et al. [20,22]. Main properties of the torus are listed in Table 4. In this study, only operational conditions are considered.

Table 4 Properties of the torus in the STC concept [22]

Item	Unit	Value
Outer diameter	[m]	20
Inner diameter	[m]	8
Draft	[m]	2
Height	[m]	8
Displacement	[m^3]	408
Mass	[ton]	418
COM location below MSL	[m]	-0.9
Mass moment of inertia in roll and pitch, I_{XX} and I_{YY}	[ton·m^2]	1.076×10^4
Mass moment of inertia in yaw, I_{ZZ}	[ton·m^2]	2.056×10^4

2.3 Connection between the torus and spar buoy

The coupled connections between the torus and spar structure include three critical components, i.e., the bearing system, end stop system, and power take-off system, as shown in Fig. 3. This subsection gives a brief description of these three components, Details of the connection system are described in Muliawan et al. [22].

The bearing system, as illustrated in Fig. 3(a), mainly controls the relative motion and transfers the coupled forces between the torus and the spar buoy. Several wheels are attached to the torus so that it can slide freely along the surface of spar buoy in heave direction. In addition, the other degrees of freedom of the relative motion between these two floaters are constrained by the bearing system.

The end stop system, as shown in Fig. 3(b), restricts the maximum relative heave motion between the torus and the spar buoy. It is used as a protective mechanism to avoid excessive relative heave motion in a hazardous sea state. This system contains two springs that are installed separately on the upper and lower ends of the system. The relative end stop distance is determined from the coupled force between these two floaters, and a +/- 3m distance is assigned in this study under operational conditions based on Muliawan et al. [22]'s recommendation . The properties of the end stop springs are given in Table 5.

The PTO system, as demonstrated in Fig. 3(c), is the key component of the wave energy converter. It absorbs the wave energy through the relative heave motion between the torus and the spar buoy. It is essentially a hydraulic cylinder which connects the torus and the spar structure. When the waves push the torus to slide along the spar, the relative heave motion forces the piston to move back and forth. The pressurized fluids inside the cylinder will drive the generator to capture wave energy. In this study, the power take-off system is simplified by introducing a linear PTO damper and a linear PTO stiffness, as shown in [22]. The properties of the power take-off system are summarized in Table 5.

Table 5. Properties of the coupled connections between the torus and the spar [20,22]

Item	Unit	Value
Stiffness upper end stop spring	[kN/m]	10^6
Stiffness lower end stop spring	[kN/m]	10^6
PTO damping coefficient	[kN·s/m]	8000
PTO stiffness coefficient	[kN/m]	10

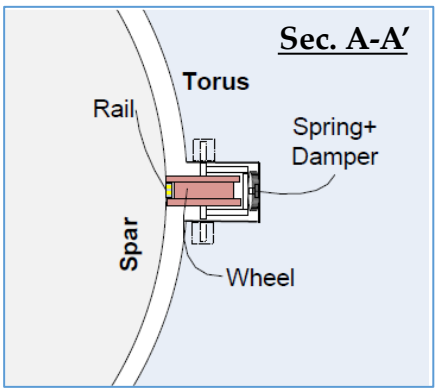

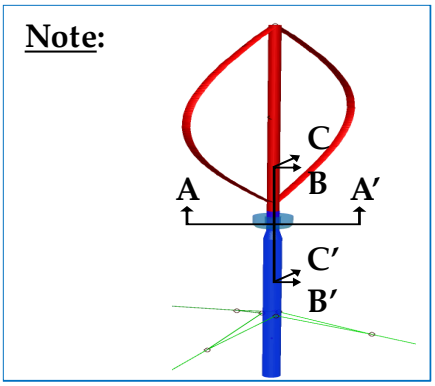

(a)

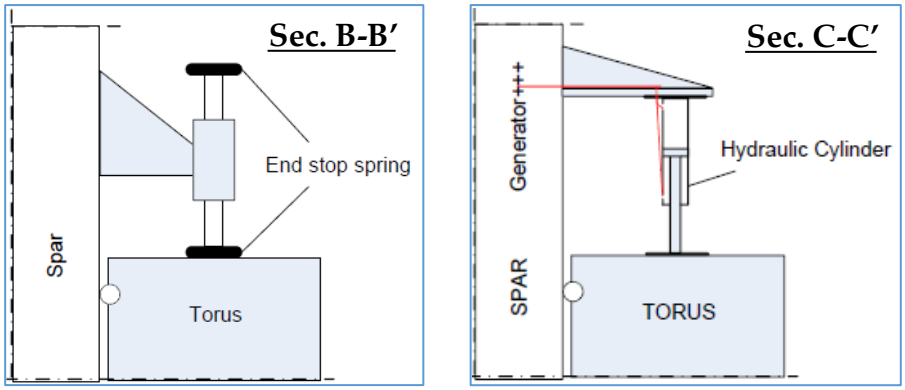

(b) (c)

Fig. 3 The coupled connection between the torus and the spar buoy: (a) Bearing system; (b) End stop system; (c) PTO system [20,22].

3 Numerical modeling of the combined concept

Numerical analysis of the combined concept requires a fully coupled simulation tool that can account for the hydrodynamic loads on the spar and torus, aerodynamic loads on the rotor, structural flexibility, controller dynamics, mooring system dynamics and mechanical and hydrodynamic couplings between the spar and torus. This can be achieved by applying the SIMO-RIFLEX-DMS, a time domain fully coupled aero-hydro-servo-elastic simulation tool. A flowchart is shown in Fig. 4 [8]. This simulation tool integrates three codes: SIMO, RIFLEX and DMS. SIMO and RIFLEX are developed by SINTEF Ocean and are widely used in the offshore oil and gas and wind industries. SIMO calculates the hydrodynamic loads on the floating structures; RIFLEX is a nonlinear finite element solver for estimating structural responses, and it also provides links to the DMS code and an external controller; DMS computes the aerodynamic loads on the blades. The external controller is used to regulate the rotational speed of the rotor. This simulation tool has been verified by a series of code-to-code comparisons against HAWC2 and SIMO-RIFLEX-AC [9].

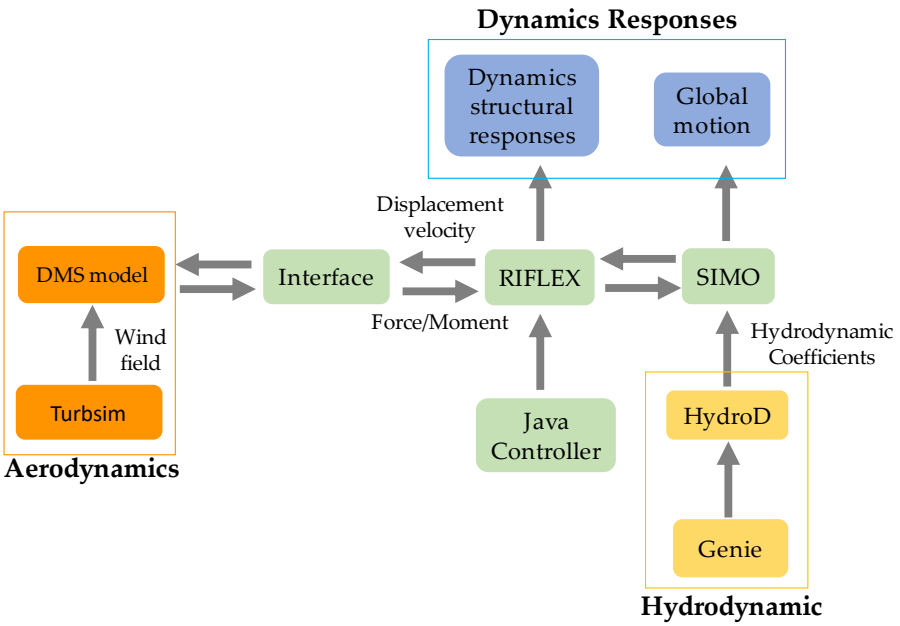

Fig. 4 Computational flowchart for fully coupled modeling and analysis of the combined concept (reproduced from Wang [8]).

3.1 Hydrodynamics

Two floating structures, i.e., the spar and the torus, are modeled as rigid bodies in this study. Hydrodynamic loads on the spar and torus are considered by a combination of potential flow theory and Morison's equation. Hydrodynamic coefficients, such as added mass, potential damping and first-order wave excitation forces, are first estimated in the frequency domain by a panel model according to the potential flow theory for both the spar and torus. Hydrodynamic interactions between the spar and the torus are taken into consideration. The PTO stiffness and damping are modeled when calculating the hydrodynamic coefficients. These hydrodynamic coefficients are then applied in the time domain by using the convolution technique [30]. Viscous forces on the spar and torus are incorporated through Morison's equation by only considering the drag term. Additionally, second-order difference-frequency forces on the spar and torus are also considered by applying the Newman's approximation.

3.2 Aerodynamics

The aerodynamic loads on the blades are calculated according to the improved Double Multiple-Streamtube (DMS) theory [31]. The DMS model accounts for the effect of variation in the Reynolds number and incorporates the effect of dynamic stall using the Beddoes-Leishman dynamic stall model. In the DMS model, the relative velocity seen at a blade section is the vector sum of the incoming wind

velocity, the induced velocity and subtracting the velocities due to the rotor rotation, platform motion and blade elastic deformation. The aerodynamic code DMS is validated by comparison with experimental results [31]. The aerodynamic load acting the tower is neglected in the present study.

3.3 Structural and mooring line dynamics

Structural dynamics are considered based on nonlinear finite element method in RIFLEX. The spar and torus are considered as rigid bodies. The blades, tower and shaft are modeled as nonlinear beam elements, while the mooring lines are represented by nonlinear bar elements. A very short tower is used to connect the rotating shaft and the spar buoy through a flexible joint. Flexible joint is a constraint element with negligible length and mass that enables the modeling of structural joints. It uses a master-slave formulation to eliminate fixed degrees of freedom. For the flexible joint used in this study, the element is able to rotate about the local axial axis of the tower with a constant stiffness of 5 kNm/deg. Rotation about the other two directions are fixed. The dynamic equations are solved in time domain by using the Newmark-β method (β=0.256, γ=0.505). Structural damping is also included by applying the global Rayleigh damping for all flexible finite elements.

3.4 Control system dynamics

The rotor considered has a fixed blade pitch angle. Hence, a generator torque controller based on the proportional integral (PI) control algorithm is used to regulate the rotor rotational speed. The controller was initially developed by Wang et al. [7] and further improved by Cheng et al. [3]. It aims to maximize the power capture for the wind speed below the rated speed and maintain the power production approximately constant for the wind speed above the rated speed. This control strategy has been applied in many research studies [3,11,32]. Here the control strategy used in the present study is only briefly described, and the detailed information is described in Cheng et al. [9].

The measured rotational speed is first filtered through a low-pass filter. The objective of this PI controller is to minimize the error between the measured and filtered rotational speed Ω_{mes} and the reference rotational speed Ω_{ref},

$$\Delta\Omega = \Omega_{\mathrm{mes}} - \Omega_{\mathrm{ref}} \tag{1}$$

in which the reference rotational speed is defined as illustrated in Fig. 5. The rotational speed error $\Delta\Omega$ is then fed through the PI path to update the required electric torque, as follows

$$T_q(t) = K_G\left(K_P\Delta\,\Omega\,(\mathrm{t}) + \mathrm{K_I}\int_0^t \Delta\,\Omega\,(\tau)d\tau\right) \quad (2)$$

where K_G is the generator stiffness, and K_P and K_I are the proportional and integral gains, respectively. The updated electric torque is thus applied to minimize the rotational speed error. In this study, $K_G = 1.5 \times 10^9 Nms/rad$, $K_P = 0.06$ and $K_I = 5 \times 10^{-4}$.

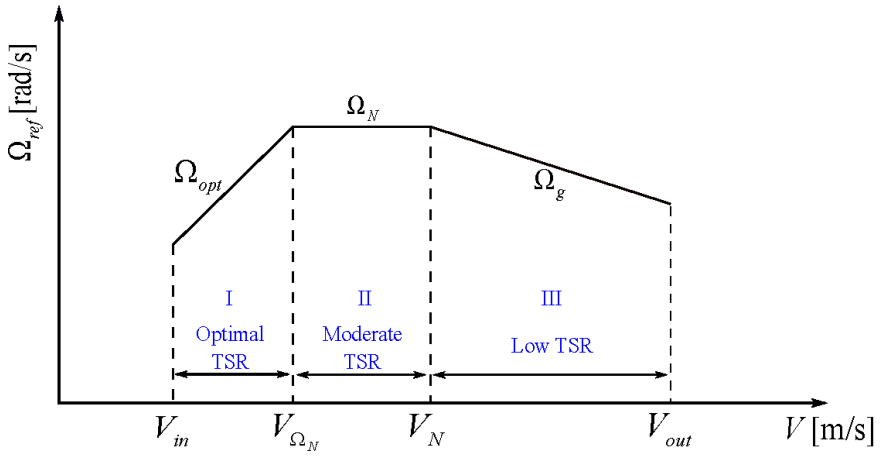

Fig.5 The relationship between the reference rotor rotational speed and the wind speed for the controller considered. V_{in}, V_N and V_{out} are the cut-in, rated, and cut-out wind speed, respectively; V_{Ω_N} is the wind speed for the rated rotational speed; Ω_N is the rated rotational speed; Ω_{opt} is the optimal rotational speed that can maximize the power capture; Ω_g is the rotational speed that can hold the mean generator power approximately constant. (reproduced from Cheng et al. [9]).

3.5 Mechanical connection between the spar and torus

The connection between the spar and the torus should allow relative motion in heave but restrain relative motions in other directions. In other words, the spar and the torus should move together in surge, sway, roll pitch and yaw. These connections are modeled using features available in SIMO, including the docking cone feature and fender feature. Detailed modeling of the mechanical connections is described by Muliawan et al. [22].

3.6 Power take-off (PTO) of wave energy converter

In the present study, the PTO system connecting the spar and the torus is simplified as an ideal linear damper with coefficient B_{PTO} and a linear spring with stiffness coefficient K_{PTO}. This model will cause internal forces in the system, which can be expressed as

$$F_{int} = B_{PTO}V_{rel} + K_{PTO}\eta_{rel} \quad (3)$$

in which the first item in the right-hand side related to B_{PTO} is proportional to the relative velocity V_{rel}, and the second item in the right-hand side related to K_{PTO} is proportional to relative heave motion η_{rel}. Moreover, the wave power absorbed by the WEC is a function of the damping coefficient and the relative velocity and can be written as

$$P_{WEC} = B_{PTO}V_{rel}^2 \quad (4)$$

Eq. (4) indicates that a higher damping coefficient B_{PTO} and a larger relative velocity V_{rel} can result in a larger wave power. It should be noted that in Eq. (3) the damping term contributes directly to the wave energy extraction while the stiffness term contributes indirectly, because the relative motion and the relative velocity between the spar and the torus depend on the values of B_{PTO} and K_{PTO} under a given sea state.

4 Environmental conditions and load cases

Only normal operational conditions are considered in this study. A set of load cases (LCs) with turbulent wind and irregular waves are chosen to evaluate the power performance and dynamic responses of the combined concept. The turbulent wind and irregular waves are correlated and directionally aligned.

The turbulent wind fields are generated by using the TurbSim program [33] according to the Kaimal turbulence model defined in IEC 61400-1 Class C [34]. The wind shear is also considered by applying the power law, in which the wind profile $U_w(z)$ is the average wind speed as a function of height z above the mean sea level (MSL), as follows:

$$U_w(z) = U_{ref}\left(\frac{z}{z_{ref}}\right)^{\alpha} \quad (5)$$

where U_{ref} is the reference wind speed, z_{ref} the height of reference wind speed and α the power law exponent. The value of z_{ref} was set to 79.78m and α was set to 0.14 in this study. The irregular waves are modeled by the JONSWAP spectrum with given significant wave height H_s and peak period T_p.

The environmental conditions are determined based on the calculation of correlated wind and waves at the Statfjord site in the Northern North Sea. In this area, a joint distribution for wind and wave was proposed by Johannessen et al. [35] as follows

$$f_{U_{10}H_sT_p}(u_{10}, h_s, t_p) = f_{U_{10}}(u_{10}) \cdot f_{H_s|U_{10}}(h_s|u_{10}) \cdot f_{T_p|H_sU_{10}}(t_p|h_s, u_{10}) \quad (6)$$

The joint distribution is the product of a marginal distribution of wind speed U_{10}, a conditional distribution of H_s for given U_{10}, and a conditional distribution of T_p for given H_s and U_{10}. Here U_{10} is defined as the 1-hour mean wind speed at 10m height. At the selected site, the marginal distribution of U_{10} is described by a two-parameter Weibull distribution and is given by

$$F_{U_{10}}(u_{10}) = 1 - \exp\left\{-\left(\frac{u_{10}}{\beta_1}\right)^{\alpha_1}\right\} \quad (7)$$

where α_1=1.708and β_1=8.426 are the shape and scale parameters, respectively. In this study, the wind speed U_w at a reference height of 79.78m is considered and given; hence, the corresponding U_{10} can be found through the power of law in Eq. (5).

The conditional distribution of significant wave height H_s for given U_{10} also follows as a two-parameter Weibull distribution. The expected value of significant wave height is given as follows

$$\mathrm{E}(H_s) = \beta_2 \Gamma\left(\frac{1}{\alpha_2} + 1\right) \quad (8)$$

where $\alpha_2 = 2 + 0.135u_{10}$ and $\beta_2 = 1.8 + 0.1{u_{10}}^{1.322}$ are the shape and scale parameters, respectively. Johannessen et al. [35] recommended that a log-normal distribution is suitable for the conditional distribution of spectral peak period T_p for given H_s and U_{10} in this site. The expected value can be derived as the following formula.

$$\mathrm{E}(T_p) = (4.883 + 2.68{h_s}^{0.529})\left[1 - 0.19\left(\frac{u_{10} - (1.764 + 3.426{h_s}^{0.78})}{1.764 + 3.426{h_s}^{0.78}}\right)\right] \quad (9)$$

By applying Eqs. (8-9), we can obtain a set of load cases with correlated wind and waves, as given in Table 6. For each load case, five independent simulations with random seeds are carried out. Each simulation lasts 4600s, in which the first 1000s is removed to eliminate the startup transient effect and to form a one-hour simulation. The statistical values and power spectra given in Section 5 are based on the average of five one-hour simulations, to reduce the stochastic variations.

Table 6 Load cases for the normal operational condition

Load case	U_w [m/s]	T_I [-]	H_s [m]	T_p [s]
LC1	5	0.224	2.10	9.74
LC2	10	0.157	2.88	9.98
LC3	14	0.138	3.62	10.29
LC4	18	0.127	4.44	10.66
LC5	22	0.121	5.32	11.06
LC6	25	0.117	6.02	11.38

5 Results and Discussions

5.1 Coupled motion of the spar and torus

The coupled motion, especially in heave, of the spar and torus is first studied in this section. As mentioned in Section 3.5, the coupled motions in surge, sway, roll, pitch and yaw between the spar and torus have been restrained; therefore, only the coupled heave motion can affect and contribute to the wave power production.

A comparison of time history of the heave motion between the spar and the torus under LC3 is plotted in Fig. 6(a). A damping coefficient B_{PTO}=8000 kN·s/m and a stiffness coefficient K_{PTO}=10 kN/m, which are determined by a parameter study presented in Section 5.2, are used to model the PTO system during the simulation. Basically, both the spar and the torus move together in heave but with a small phase difference. The heave motion of the spar follows that of the torus. The reason is that the first order wave excitation force in heave of the torus is significantly larger than that of the spar, as shown in Fig. 6(b). As a result, the torus carries the spar to move vertically, and the PTO system makes use of the relative heave motion to extract wave energy. It can be observed from Fig. 6(b) that the heave wave excitation force of the spar and the torus are about 180 degree out of phase with each other. This is due to due to the selection of damping and stiffness parameters in the PTO system. The situation might be different if a different combination of damping and stiffness parameters is used. The variations of torus motion in heave are slightly more significant than that of the spar, whereas their difference is smaller than 3m due to the deployment of the end stop system. A similar phenomenon can also be found in the heave velocity of the torus and the spar under LC3, as shown in Fig. 6(c).

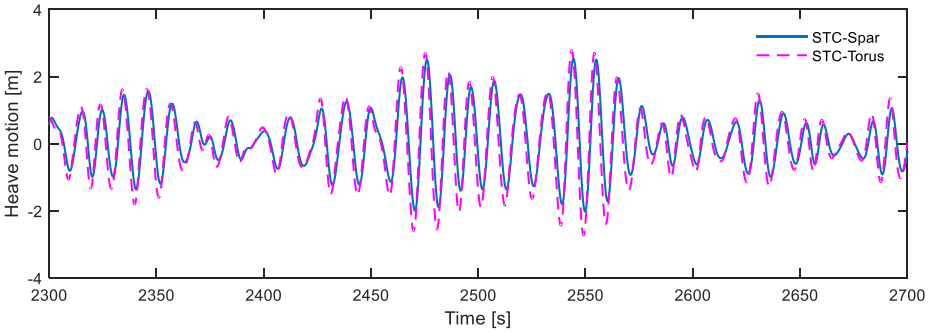

(a) Heave motion of the spar and torus

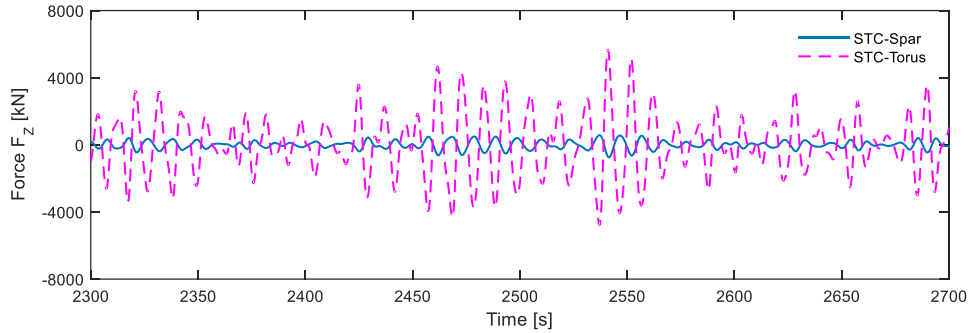

(b) First-order wave excitation force in heave

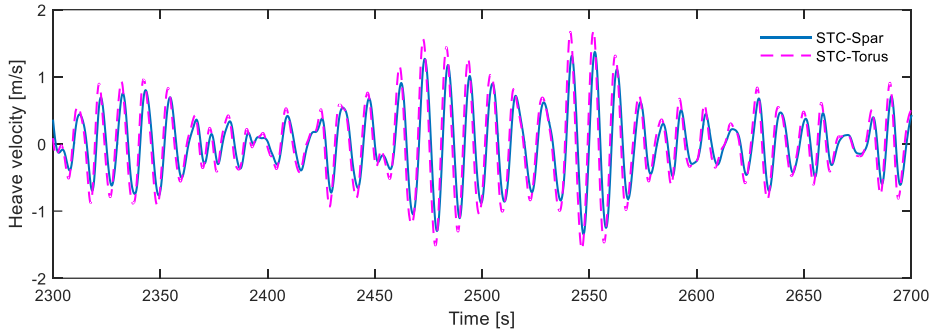

(c) Heave velocity of the spar and torus

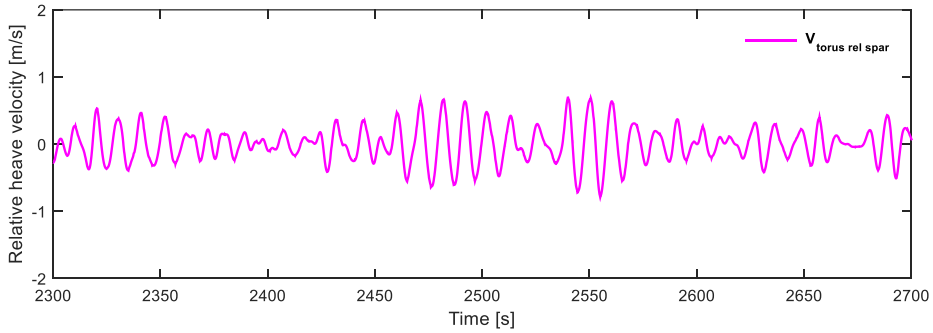

(d) Relative heave velocity between the spar and torus

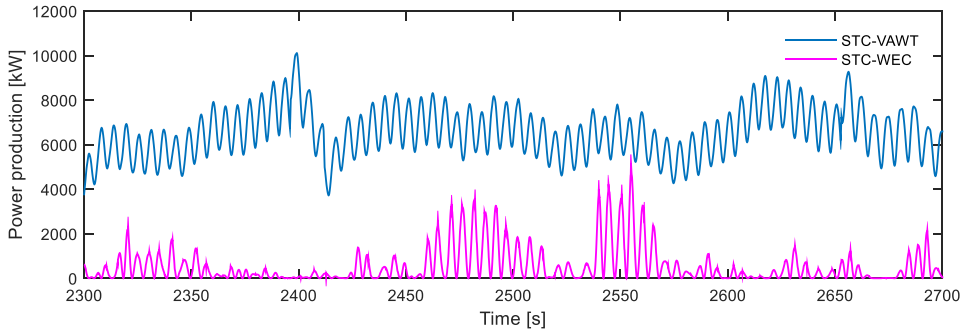

(e) Wind and wave power production

Fig. 6 Time histories of (a) heave motion (b) First order wave excitation force in heave (c) heave velocity of the spar and the torus, (d) relative heave velocity between the spar and torus, and (e) wind and wave power production for the combined STC concept under load case LC3.

The relative heave velocity between the spar and the torus is plotted in Fig. 6(d). The corresponding wave power captured by the PTO system is shown in Fig. 6(e). A larger relative heave velocity leads to

a larger wave power production. In addition, the wind power production from the Darrieus rotor is also shown in Fig. 6(e). It can be found that the wind power production is much larger than the wave power production. The wind power has a prominent variation with a period of about 11s, which is due to the periodic aerodynamic loads acting on the rotor.

5.2 Power performance of the combined concept

The power performance of the combined concept, including wind power, wave power and annual power production, is evaluated in this section. Since the wave power production is sensitive to the damping and stiffness coefficients in the PTO system, a parameter study of the PTO parameters is conducted first. It should be noted that only a preliminary parameter study is performed here to identify the optimum parameters, because this study aims to demonstrate the power performance and dynamic response characteristics of the novel combined wind and wave energy concept.

5.2.1 Parameter study of PTO parameters

The linear spring and linear damper of the PTO system dominate the relative heave motion between the torus and the spar. If the spring is too stiff, i.e., stiffness coefficient K_{PTO} is too large, the torus and the spar will behave like one rigid body and move synchronously in heave, leading to very small wave power absorption. Hence, an appropriate stiffness coefficient is necessary. Here we assume a stiffness coefficient of K_{PTO}=10 kN/m, based on relevant studies by Muliawan et al. [22].

Compared to the stiffness coefficient, the damping coefficient directly controls the wave power absorption. A parameter study of the damping coefficient under selected load cases is carried out. Three damping coefficients, i.e., B_{PTO}=2000, 8000 and 12000 kNs/m, are considered. The mean value and standard deviation of wave power production are shown in Fig. 7. The result indicates that the damping coefficient B_{PTO}=8000 kNs/m gives larger wave power production than the others. Therefore, the stiffness coefficient K_{PTO}=10 kN/m and damping coefficient B_{PTO}=8000 kNs/m are used in this study.

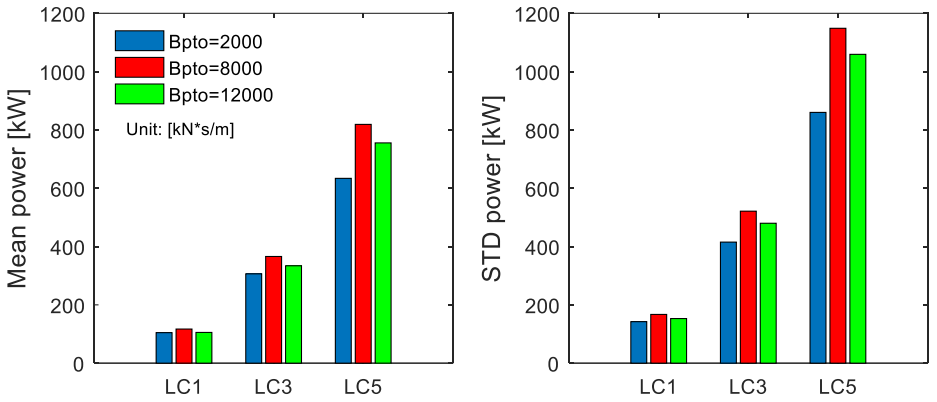

(**a**) Mean value (**b**) Standard deviation

Fig. 7 The mean value and standard deviation of wave power production with different damping coefficient in the PTO system and under selected load cases.

5.2.2 Annual power production

The mean value and standard deviation of the wind power performance of the combined concept under all load cases are shown in Fig. 8. In general, the mean wind power production increases with the wind speed below the rated wind speed (LC3), whereas it maintains an approximately constant as the wind speed is higher than the rated speed. This is due to the application of the PI-based generator torque controller, as introduced in Section 3.4.

Fig. 8 also compares the wind power performance between the combined concept and the spar-type VAWT under different load cases. Good agreements are found in both the mean value and standard deviation of wind power production for the two concepts, which implies that introducing the torus for wave energy absorption does not affect the wind power production.

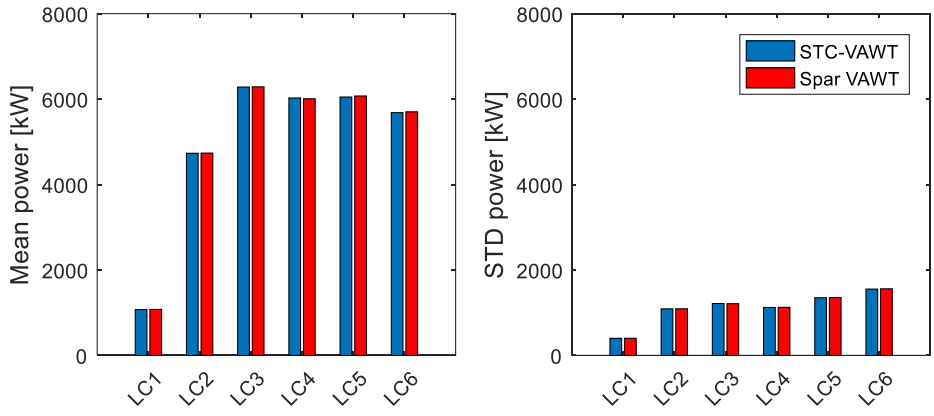

(**a**) Mean value (**b**) Standard deviation

Fig. 8 A comparison of (a) mean value and (b) standard deviation of wind power production between the combined STC concept and the spar-type VAWT under all load cases.

The wind and wave power production by the combined concept is of great interest and studied. Fig. 9 demonstrates the mean value and standard deviation of wind and wave power production in the combined concept under all load cases. It can be found that the wave power production is strongly correlated with the environmental conditions. Both the mean value and standard deviation of wave power production increases as the significant wave height increases. In general, the VAWT produces much more power than the WEC in the combined concept.

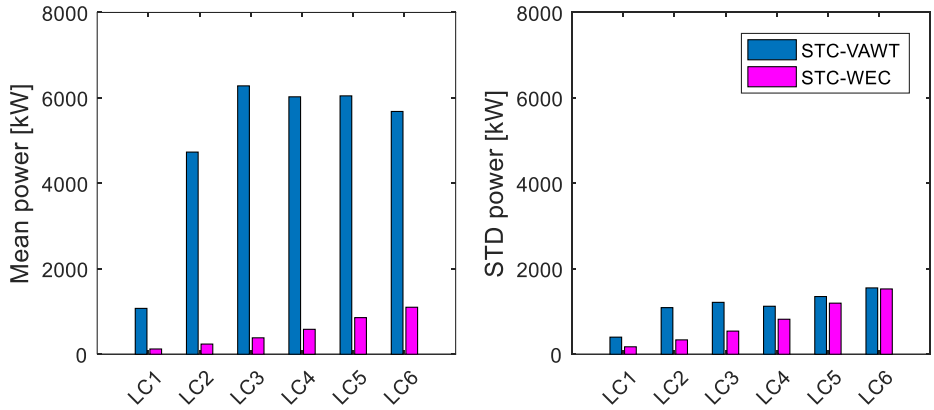

(**a**) Mean value (**b**) Standard deviation

Fig. 9 A comparison of (a) mean value and (b) standard deviation of wave and wind power production in the combined STC concept under all load cases.

The wind and wave power production is further studied by estimating the annual power production. The annual power production is determined based on the probabilistic distribution of wind speed in the site considered. The marginal distribution of one-hour mean wind speed at 79.78m can be derived based on Eqs. (5) and (7).

The annual power production can be roughly estimated as the summation of the product of mean power and the corresponding probability of mean wind speed within one year. The availability of the combined concept over one year is assumed to be 1. Since the wind and wave conditions in each load cases are correlated, the same probability from marginal distribution of wind speed can be applied for estimating annual wand power production and annual wave power production.

Fig. 10 compares the annual power production performance of the spar-type VAWT and the combined concept. Generally, the estimated result shows a good agreement between the only spar-type VAWT and the wind power production in the combined concept. The annual wave power production of the combined concept is about 2.2 GWh, which is approximately 7% of the annual wind power production.

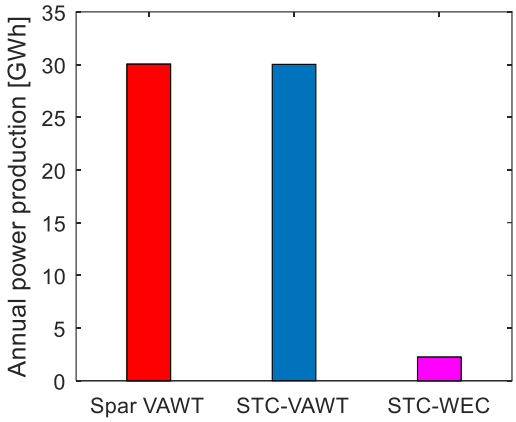

Fig. 10 Annual power production for the spar-type VAWT and the combined STC concept.

5.3 Dynamic responses of the combined concept

5.3.1 Aerodynamic loads

The prominent aerodynamic loads on a vertical axis wind turbine (VAWT) involve thrust, lateral force and aerodynamic torque. The direction of thrust and lateral force is parallel and normal to the wind flow, respectively. For a two-bladed Darrieus rotor, the aerodynamic loads vary twice per revolution (2P) due to the variation of the angle of attack at different azimuthal angles [9]. The mean value and standard deviation of the thrust, lateral force and aerodynamic torque of the combined concept under all load cases are plotted in Fig. 11. In principle, all these aerodynamic loads increase as the wind speed increases.

The statistical comparisons of aerodynamic loads between the combined concept and the spar-type VAWT are also shown in Fig. 11. For both mean values and standard deviations, good agreements between the combined concept and the spar-type VAWT are observed. This outcome is expectable since the same VAWT is implemented in both concepts. The result also leads to the very close wind power production of the combined concept and the spar-type VAWT, as aforementioned in Fig. 8.

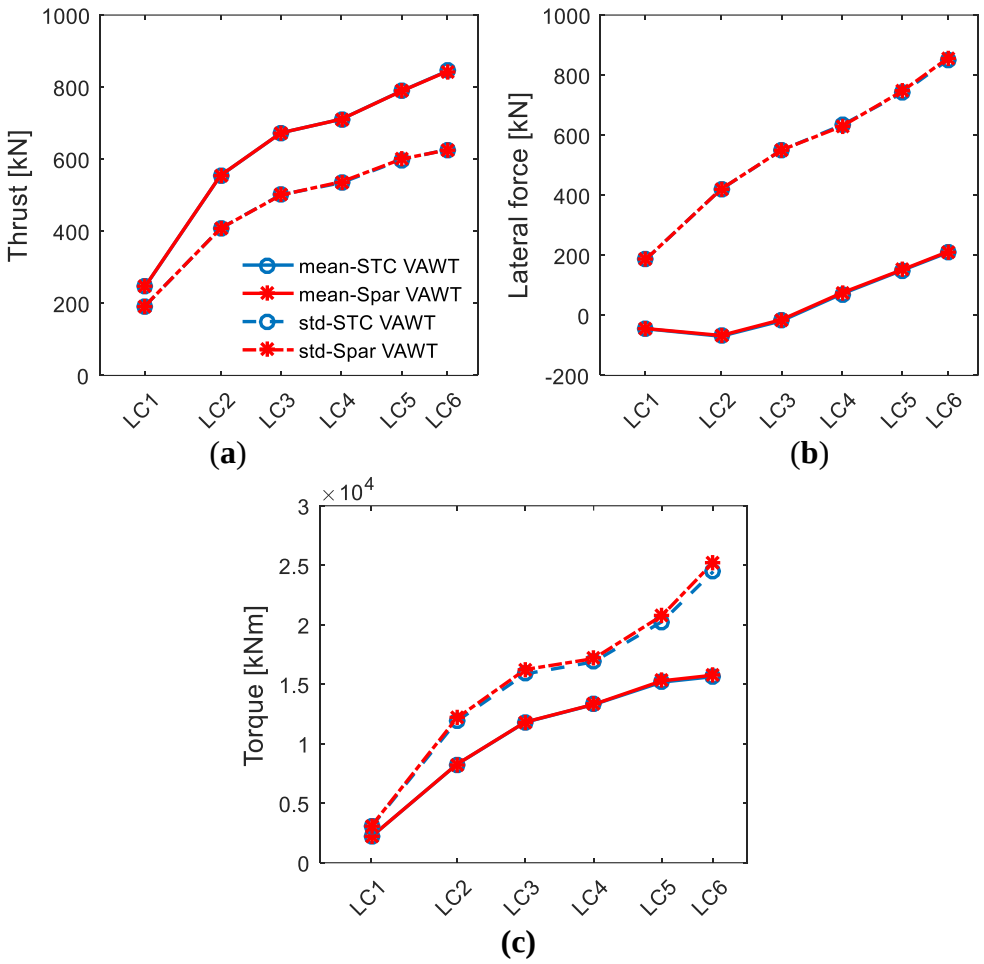

Fig. 11 Statistical comparisons of aerodynamic loads between the combined STC concept and the spar-type VAWT under all loading cases: (a) thrust; (b) lateral force; (c) aerodynamic torque.

5.3.2 Floater motions

Motion of the combined concept is addressed in this section. The combined concept consists of two floaters, i.e., spar and torus. The mean value and standard deviation of motions of the spar and torus under all load cases are analyzed, as shown in Fig. 12. It can be found that the surge motion of the spar coincides with that of the torus motion. This is due to the mechanical connection and PTO system described in Sections 3.5 and 3.6. The spar and torus move together except for heave motion. Regarding the heave motion, the mean values are close to zero for both the spar and torus, but the torus has a larger standard deviation than the spar, especially in load cases with larger significant wave height. In addition, the standard deviations of heave motion for both the spar and torus increase with the increase of turbulent wind and irregular waves.

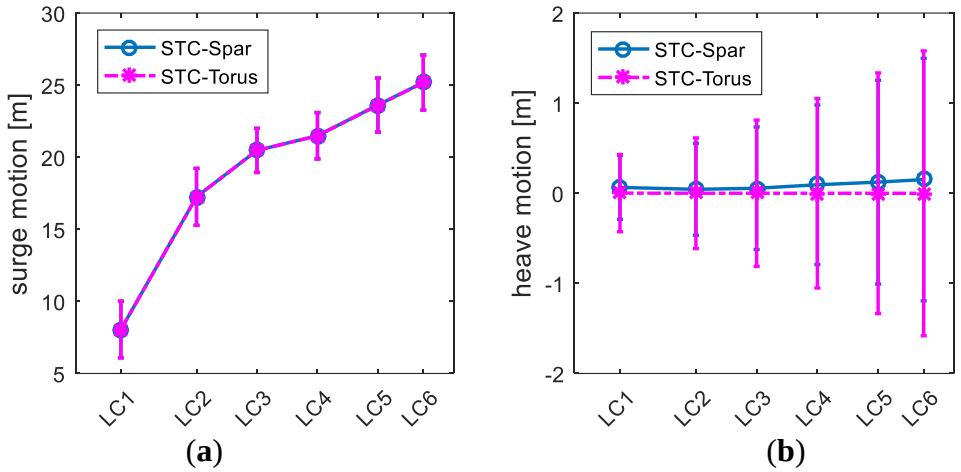

Fig. 12 The mean floater motion of the spar and the torus with the error bars representing the standard deviations in the combined STC concept: (a) Surge; (b) Heave.

The power spectral analysis is used to further reveal the contribution of different frequency components. Fig. 13 displays the power spectra of surge and heave motions of the spar and the torus in the combined concept under load case LC3. It can be found that the spar and torus have identical power spectra in surge motion. The surge power spectrum is dominated by the surge resonant response, wave frequency response and 2P response. As a contrast, the heave power spectra of the spar and the torus differ and are mainly dominated by the wave frequency response and heave resonant response.

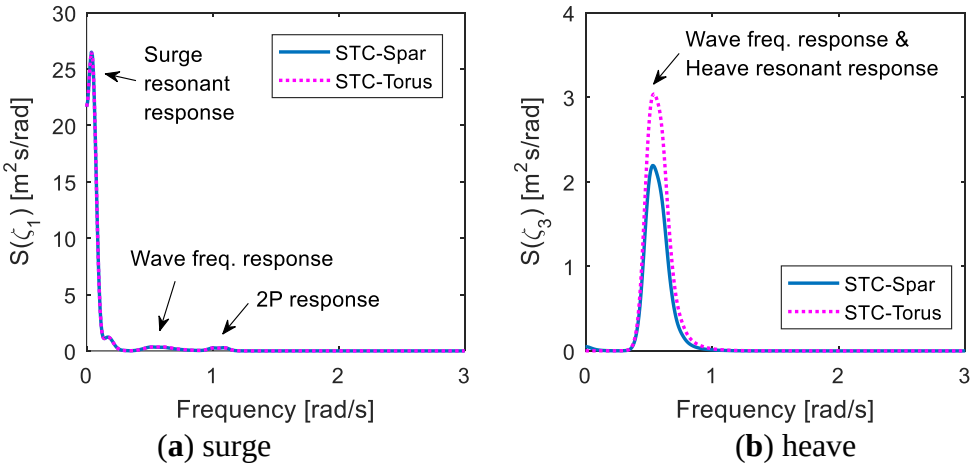

Fig. 13 Power spectra of surge and heave motions of the spar and the torus in the combined STC concept under load case LC3.

Motion of the spar in the combined concept is also compared to that of the spar-type VAWT to evaluate the effect of torus on the motion of the spar. The mean value and standard deviation of motions

in surge, sway, heave and pitch of the spar floaters are shown in Fig. 14. In general, introducing the torus gives rise to a slight decrease in the mean value and standard deviation of surge, sway and pitch motions. This is mainly because the torus experiences large resistance near the mean water level and provides an additional damping effect to mitigate the motions in surge, sway and pitch.

However, the standard deviation of the heave motion for the combined concept is significantly larger than that of the spar-type VAWT. This is because introducing the torus changes the natural period of heave motion for the whole system. The heave natural period of the spar-type VAWT is about 27.3s. When the torus is added, the heave natural period of the combined concept is changed to be approximately 12.2s, which is well within the ocean wave periods. Heave resonant response is thus excited for the combined concept, leading to significantly larger heave standard deviation. However, the larger heave motion does not affect the wind energy production of the combined concept, as shown in Fig. 8. Moreover, the torus makes use of the relatively large heave motion to capture more wave energy, which is favorable from maximizing energy capturing point of view.

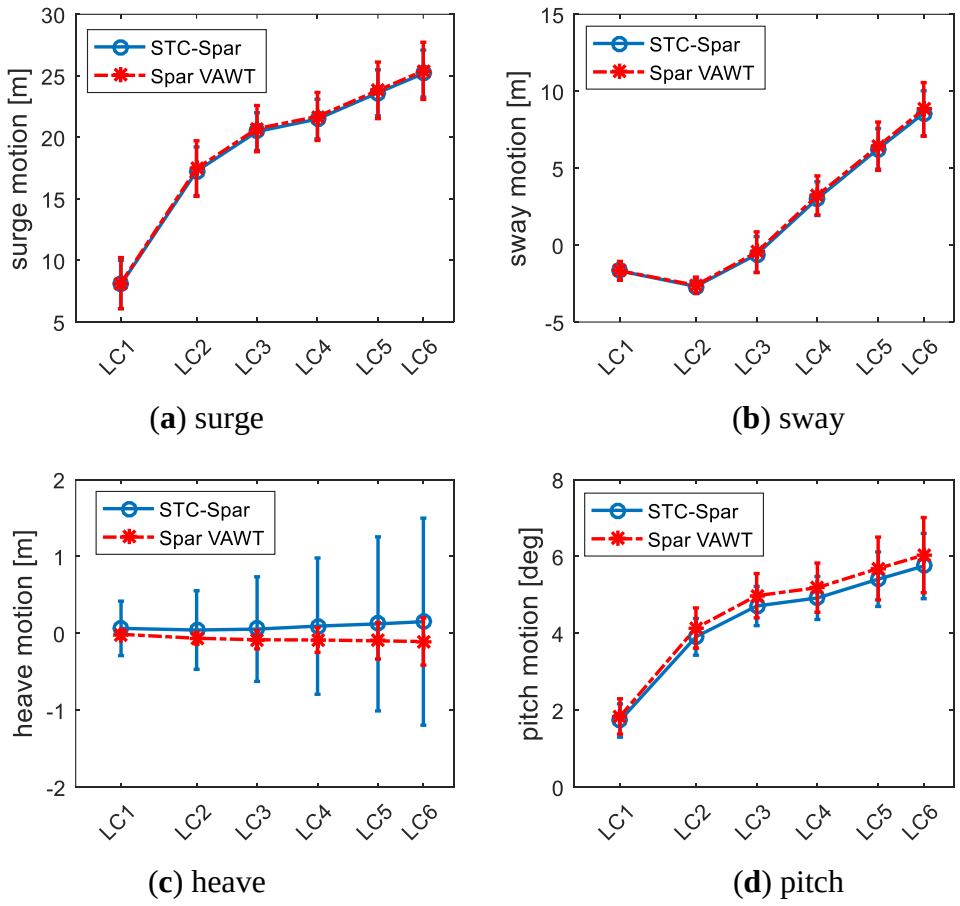

Fig. 14 Comparison of mean values and standard deviations of motions of the spar between the combined STC concept and the spar-type VAWT under all load cases. (a) Surge; (b) Sway; (c) Heave; (d) Pitch.

The effect of the torus is also studied by power spectral analysis. Power spectra of spar motion between the combined concept and the spar-type VAWT under load case LC3 are shown in Fig. 15. The power spectra of motions in surge, sway and pitch between the combined concept and the spar-type VAWT are very close, except at the low-frequency range. These low-frequency responses are due to turbulent wind forces and second-order difference-frequency wave excitation forces. According to Fig. 11, the wind excitation forces between the two concepts are very similar, since identical turbulent wind fields are applied. The combined concept has a relatively larger second-order wave excitation force because of the presence of the torus. However, low-frequency motions in surge, sway and pitch of the combined concept are in contrast smaller than those of the spar-type VAWT. This is because the torus also contributes to the damping and helps to mitigate the low-frequency motions in surge, sway and pitch. Regarding the heave spectra of the spar floater in the combined concept and the spar-type VAWT, they differ significantly as shown in Fig. 15(c). The difference mainly comes from the fact that the heave resonant response is greatly excited in the combined concept.

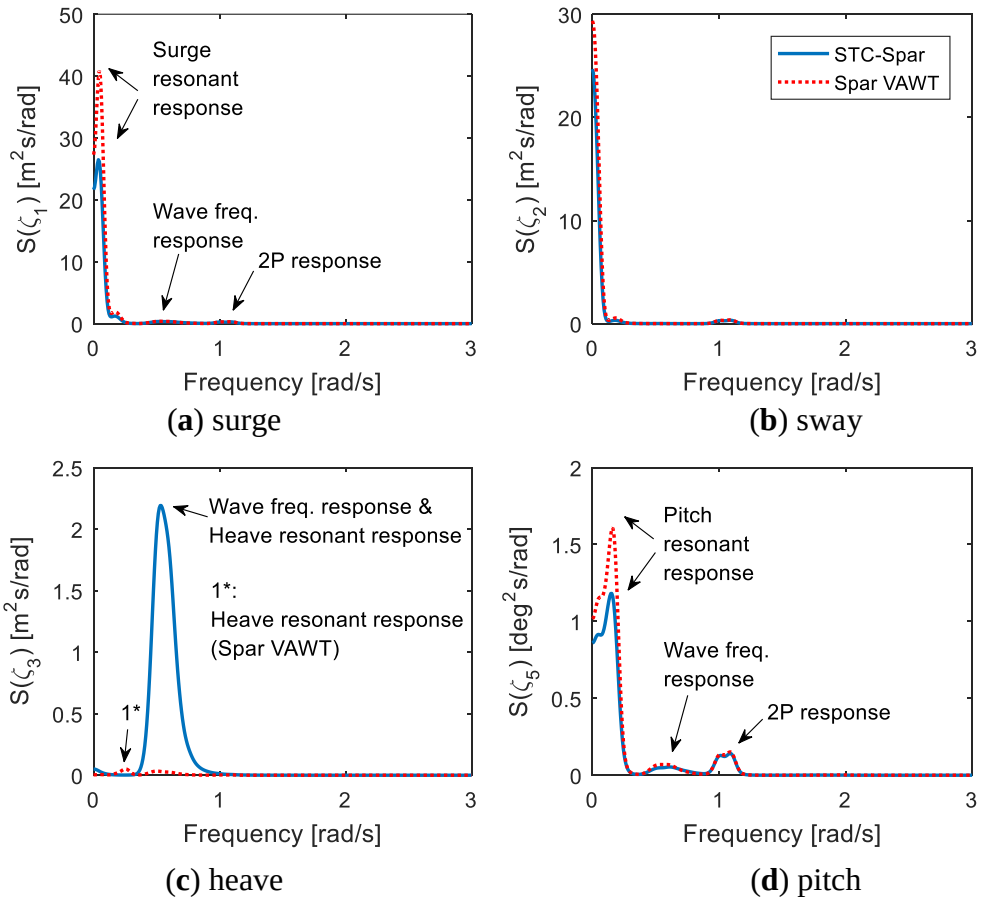

Fig. 15 Comparison of motion spectra of the spar between the combined STC concept and the spar-type VAWT under load case LC3. (a) Surge; (b) Sway; (c) Heave; (d) Pitch.

5.3.3 Tower base bending moment

The tower base bending moment is mainly caused by the aerodynamic loads on the rotor, by the self-weight of the rotor due to tower tilt, and by the wave excitation loads acting on the platform. The tower base fore-aft and side–side bending moments, which are respectively parallel and perpendicular to the wind flow, are considered in this study. The mean values and standard deviations of the tower base bending moment between the combined concept and the spar-type VAWT under all load cases are compared, as shown in Fig. 16. In general, the mean values of tower base fore-aft and side-side bending moments between the two concepts are very close. The combined concept gives a slightly smaller mean value in the tower base both fore-aft and side-side bending moments than the spar-type VAWT.

However, the combined concept gives larger standard deviations of tower base fore-aft and side-side bending moments than the spar-type VAWT. Difference in standard deviations is revealed by the power spectral analysis. Fig. 17 shows the power spectra of tower base fore-aft and side-side bending moments of the combined concept and the spar-type VAWT under LC3. It can be found that both tower base fore-aft and side-side bending moment spectra are dominated by the 2P response, which is mainly induced by periodic 2P aerodynamic loads. Moreover, the combined concept has a slight larger 2P response than the spar-type VAWT.

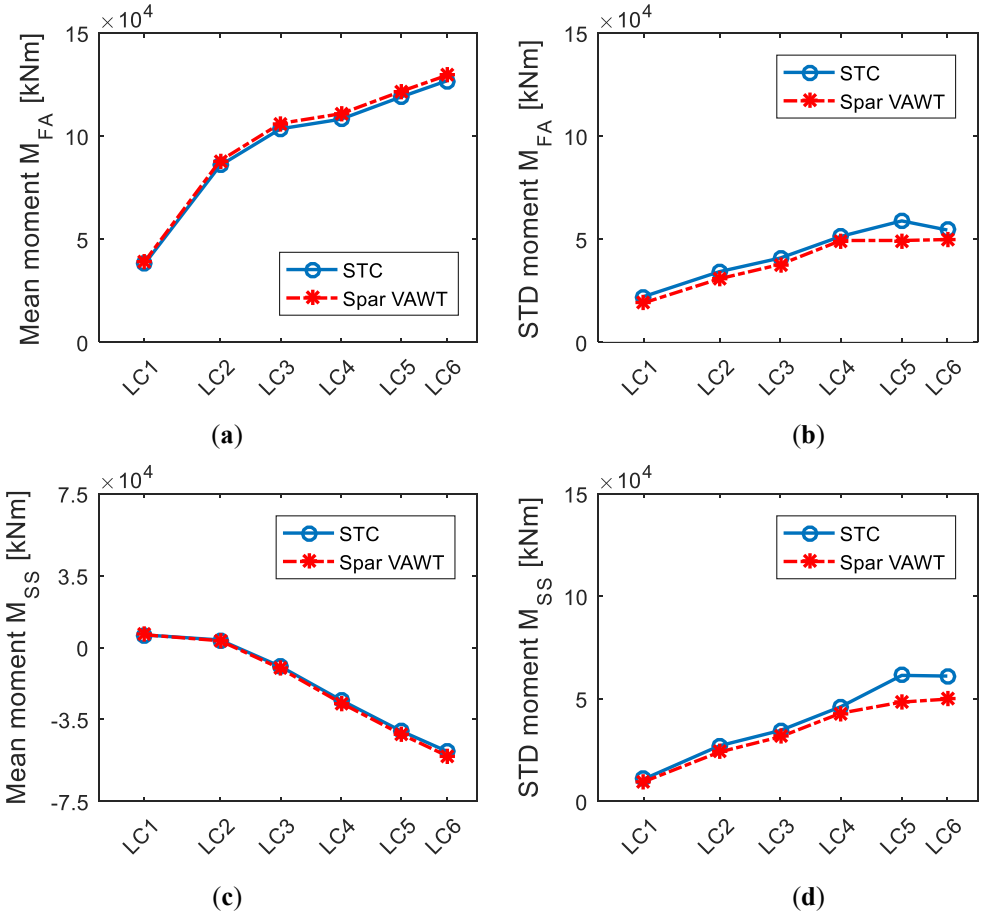

Fig. 16 Comparison of mean values and standard deviations of tower base fore-aft and side-side bending moments between the combined STC concept and the spar-type VAWT under all load cases: (a) Mean values of tower base fore-aft bending moment; (b) Standard deviations of tower base fore-aft bending moment; (c) Mean values of tower base side–side bending moment; (d) Standard deviations of tower base side–side bending moment.

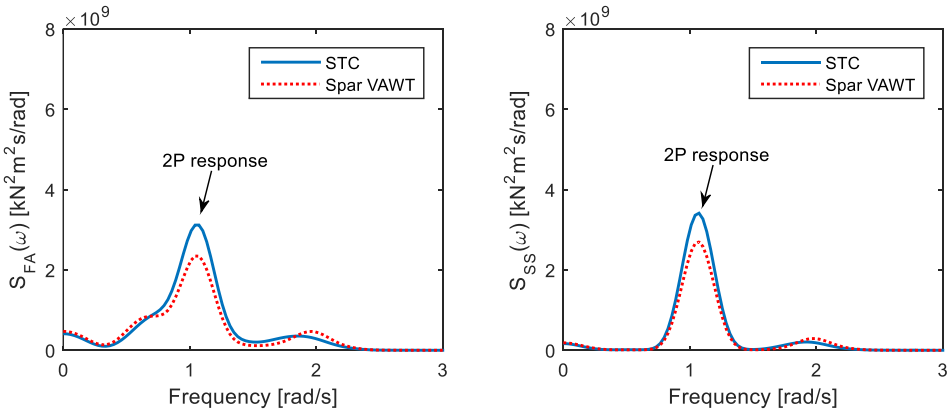

(**a**) fore-aft bending moment (**b**) side-side bending moment

Fig. 17 Comparisons of power spectra of tower base fore-aft and side-side bending moment between the combined STC concept and the spar-type VAWT under load case LC3.

5.3.4 Mooring line tension

The combined concept is moored by a catenary chain mooring system with clump weight and delta lines. Delta lines are employed to increase the yaw stiffness of the whole system. Identical mooring system is applied to the spar-type VAWT. The mooring system consists of three mooring lines, among which mooring line 1 is aligned with the wind and wave direction and is subjected to the largest tension. Tension in mooring line 1 is thus studied in this section.

The mean value and standard deviation of tension in mooring line 1 between the combined concept and the spar-type VAWT under all load cases are compared, as shown in Fig. 18. The combined concept displays a good agreement in the mean tension of mooring line 1 with the spar-type VAWT. However, it also causes slightly larger standard deviation of tension in mooring line 1. Reason for this small discrepancy is revealed by power spectral analysis, as shown in Fig. 19. For the spar-type VAWT, the power spectrum of tension in mooring line 1 is mainly dominated by low-frequency turbulent wind induced response; while for the combined concept, not only turbulent wind induced response but also wave-frequency response is dominating in the power spectrum of tension in mooring line 1. In the combined concept, the additional torus contributes to damping which mitigates the low-frequency response; at the same time, it also contributes to excitation force that causes a relatively large wave-

frequency response. As a result, introducing the additional torus cause a slight increase of standard deviation of tension in mooring line 1 in the combined concept; but such an increase is very small compared to the mean value.

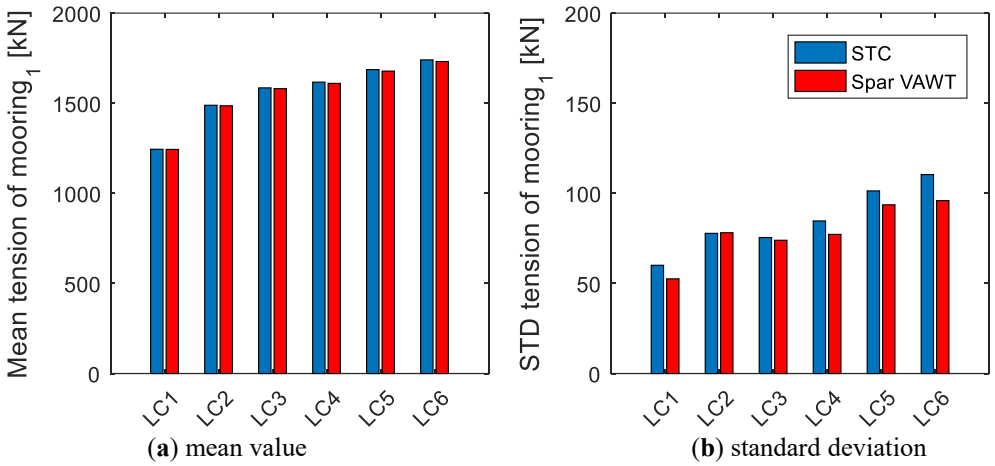

Fig. 18 Comparison of mean value and standard deviation of tension in mooring line 1 between the combined STC concept and the spar-type VAWT under all load cases.

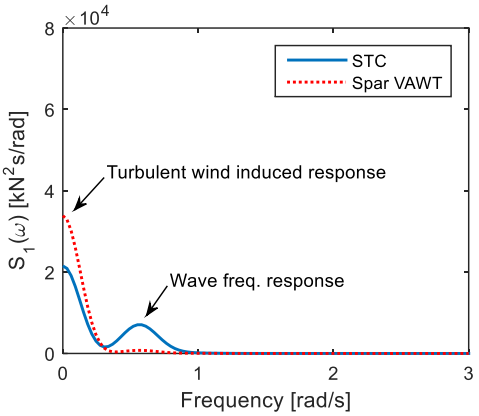

Fig. 19 Power spectrum of tension in mooring line 1 for both the combined STC concept and the spar-type VAWT under different load case LC3.

6 Conclusions

This study proposes a novel combined wind and wave energy concept STC, which is composed of a spar-type floating vertical axis wind turbine (VAWT) and a torus-shaped wave energy converter (WEC). The VAWT and WEC share the same spar buoy, mooring system and power cables, implying a reduction of capital cost. The WEC utilizes the relative heave motion between the spar and the torus to capture wave energy. Power performance and dynamic responses of the combined concept are evaluated

by conducting fully coupled time domain simulations under turbulent wind and irregular waves. Main conclusions are summarized as follows:

- Compared to spar-type VAWT, the combined concept produces more energy due to the WEC. The WEC does not affect the power production of the VAWT, and it causes about 7% increase in the total annual power production.
- Introducing the WEC does not affect the aerodynamic loads acting on the VAWT in the combined concept.
- Because of the WEC, the natural period of heave motion of the combined concept is within the ocean wave periods. Resonant heave motion is excited in the combined concept; as a result, the combined concept has much larger heave motion than the spar-type VAWT. However, such resonant heave motion has limited impacts on the dynamic responses of the whole system; in contrast, the WEC makes use of the relative large heave motion to extract wave energy.
- The WEC also introduces damping to the whole system, which helps mitigate the low-frequency responses in the surge, sway and pitch motions and mooring line tension.
- The combined concept suffers relatively larger tower base fore-aft and side-side bending moments than the spar-type VAWT, due to the increase in the 2P resonant response.

As a whole, the present study proposes a novel combined wind and wave energy concept, evaluates its power performance and reveals its dynamic response characteristics. The results demonstrate that the proposed combined concept is promising. However, it should be noted that such evaluations are only carried out in normal operational conditions. Further studies on its performance under survival conditions are to be conducted in the future. Under survival conditions, the torus is locked to the spar and the Mathieu instability might occur. Aeroelastic instability might also occur for the considered combined concept. These instability issues are of interest to be studied in the future.

Acknowledgments

The first author appreciates the support from the State Key Laboratory of Hydraulic Engineering Simulation and Safety (HESS-1710), Tianjin University, Tianjin, China. The second author would like to acknowledge the financial support from the COTech at Faculty of Science and Technology, University of Stavanger (UiS).

References

[1] Stehly T, Heimiller D, Scott G. 2016 Cost of Wind Energy Review. Tech. Rep. NREL/TP-6A20-70363,

NREL, Golden, CO, USA: 2017.

[2] Paquette J, Barone M. Innovative offshore vertical-axis wind turbine rotor project. EWEA 2012 Annu Event 2012.

[3] Cheng Z, Wang K, Gao Z, Moan T. A comparative study on dynamic responses of spar-type floating horizontal and vertical axis wind turbines. Wind Energy 2017;20:305–23. doi:10.1002/we.2007.

[4] Paulsen US, Vita L, Madsen HA, Hattel J, Ritchie E, Leban KM, et al. 1st DeepWind 5 MW Baseline design. Energy Procedia 2012;24:27–35. doi:10.1016/j.egypro.2012.06.083.

[5] Paulsen US, Borg M, Madsen HA, Pedersen TF, Hattel J, Ritchie E, et al. Outcomes of the DeepWind Conceptual Design. Energy Procedia 2015;80:329–41. doi:http://dx.doi.org/10.1016/j.egypro.2015.11.437.

[6] Borg M, Collu M. Frequency-domain characteristics of aerodynamic loads of offshore floating vertical axis wind turbines. Appl Energy 2015;155:629–36. doi:10.1016/j.apenergy.2015.06.038.

[7] Wang K, Moan T, Hansen MOL. A method for modeling of floating vertical axis wind turbine. Proc. 32th Int. Conf. Ocean. Offshore Arct. Eng., Nantes, France.: OMAE2013-10289; 2013.

[8] Wang K, Moan T, Hansen MOL. Stochastic dynamic response analysis of a floating vertical-axis wind turbine with a semi-submersible floater. Wind Energy 2016;19:1853–70. doi:10.1002/we.1955.

[9] Cheng Z, Madsen HA, Gao Z, Moan T. A fully coupled method for numerical modeling and dynamic analysis of floating vertical axis wind turbines. Renew Energy 2017;107:604–19. doi:10.1016/j.renene.2017.02.028.

[10] Cheng Z, Wang K, Gao Z, Moan T. Dynamic response analysis of three floating wind turbine concepts with a two-bladed Darrieus rotor. J Ocean Wind Energy 2015;2:213–22. doi:10.17736/jowe.2015.jcr33.

[11] Cheng Z, Madsen HA, Gao Z, Moan T. Effect of the number of blades on the dynamics of floating straight-bladed vertical axis wind turbines. Renew Energy 2017;101:1285–98. doi:10.1016/j.renene.2016.09.074.

[12] Cheng Z, Wang K, Ong MC. Assessment of performance enhancement of a semi-submersible vertical axis wind turbine with an optimized Darrieus rotor. Eng Struct 2018;167:227–40. doi:10.1016/j.engstruct.2018.04.038.

[13] Liu L, Guo Y, Zhao H, Tang Y. Motions of a 5 MW floating VAWT evaluated by numerical simulations and model tests. Ocean Eng 2017;144:21–34. doi:10.1016/J.OCEANENG.2017.08.004.

[14] French MJ. On the difficulty of inventing an economical sea wave energy converter: A personal view. Proc Inst Mech Eng Part M J Eng Marit Environ 2006;220:149–55. doi:10.1243/14750902JEME43.

[15] Babarit A, Hals J, Muliawan MJ, Kurniawan A, Moan T, Krokstad J. Numerical benchmarking study of a selection of wave energy converters. Renew Energy 2012;41:44–63. doi:10.1016/J.RENENE.2011.10.002.

[16] Muliawan MJ, Gao Z, Moan T, Babarit A. Analysis of a Two-Body Floating Wave Energy Converter With Particular Focus on the Effects of Power Take-Off and Mooring Systems on Energy Capture. J Offshore Mech Arct Eng 2013;135:031902. doi:10.1115/1.4023796.

[17] MARINA Platform n.d. http://msp-platform.eu/projects/marina-platform (accessed February 1, 2018).

[18] Michailides C, Gao Z, Moan T. Experimental study of the functionality of a semisubmersible wind turbine combined with flap-type Wave Energy Converters. Renew Energy 2016;93:675–90. doi:10.1016/j.renene.2016.03.024.

[19] Michailides C, Gao Z, Moan T. Experimental and numerical study of the response of the offshore combined wind/wave energy concept SFC in extreme environmental conditions. Mar Struct 2016;50:35–54. doi:10.1016/J.MARSTRUC.2016.06.005.

[20] Muliawan MJ, Karimirad M, Moan T, Gao Z. STC (Spar-Torus Combination): A Combined Spar-Type Floating Wind Turbine and Large Point Absorber Floating Wave Energy Converter — Promising and Challenging. Proc. ASME 2012 31st Int. Conf. Ocean. Offshore Arct. Eng., ASME; 2012, p. 667–76. doi:10.1115/OMAE2012-84272.

[21] Muliawan MJ, Karimirad M, Gao Z, Moan T. Extreme responses of a combined spar-type floating wind turbine and floating wave energy converter (STC) system with survival modes. Ocean Eng 2013;65:71–82. doi:10.1016/J.OCEANENG.2013.03.002.

[22] Muliawan MJ, Karimirad M, Moan T. Dynamic response and power performance of a combined Spar-type floating wind turbine and coaxial floating wave energy converter. Renew Energy 2013;50:47–57. doi:10.1016/J.RENENE.2012.05.025.

[23] Aubault A, Alves M, Sarmento A, Roddier D, Peiffer A. Modeling of an Oscillating Water Column on the Floating Foundation WindFloat. Vol. 5 Ocean Sp. Util. Ocean Renew. Energy, ASME; 2011, p. 235–46. doi:10.1115/OMAE2011-49014.

[24] Wan L, Gao Z, Moan T. Experimental and numerical study of hydrodynamic responses of a combined wind and wave energy converter concept in survival modes. Coast Eng 2015;104:151–69. doi:10.1016/J.COASTALENG.2015.07.001.

[25] Wan L, Gao Z, Moan T, Lugni C. Experimental and numerical comparisons of hydrodynamic responses for a combined wind and wave energy converter concept under operational conditions. Renew Energy 2016;93:87–100. doi:10.1016/J.RENENE.2016.01.087.

[26] Ren N, Gao Z, Moan T, Wan L. Long-term performance estimation of the Spar–Torus-Combination (STC) system with different survival modes. Ocean Eng 2015;108:716–28. doi:10.1016/J.OCEANENG.2015.08.013.

[27] Jonkman JM. Definition of the floating system for Phase IV of OC3. 2010.

[28] Jonkman JM, Butterfield S, Musial W, Scott G. Definition of a 5-MW reference wind turbine for offshore system development. Tech. Rep. NREL/TP-500-38060, NREL, Golden, CO, USA: 2009.

[29] Wen TR, Wang K, Cheng Z, Ong MC. Spar-Type Vertical-Axis Wind Turbines in Moderate Water Depth: A Feasibility Study. Energies 2018;11:555. doi:10.3390/en11030555.

[30] Faltinsen OM. Sea loads on ships and offshore structures. Cambridge, UK: Cambridge University Press; 1995.

[31] Wang K, Hansen MOLOL, Moan T. Model improvements for evaluating the effect of tower tilting on the aerodynamics of a vertical axis wind turbine. Wind Energy 2015;18:91–110. doi:10.1002/we.1685.

[32] Cheng Z, Madsen HA, Chai W, Gao Z, Moan T. A comparison of extreme structural responses and fatigue damage of semi-submersible type floating horizontal and vertical axis wind turbines. Renew Energy 2017;108:207–19. doi:10.1016/j.renene.2017.02.067.

[33] Jonkman BJ. TurbSim user's guide: Version 1.50. . Tech. Rep. NREL/TP-500-46198, NREL, Golden, CO, USA: 2009.

[34] IEC. International Standard 61400-1, Wind turbines, Part 1: Design requirements 2005.

[35] Johannessen K, Meling TS, Haver S. Joint distribution for wind and waves in the northern north sea. Int J Offshore Polar Eng 2002;12.